Journal of Neuroscience Methods 320 (2019) 37–43

Contents lists available at ScienceDirect

Journal of Neuroscience Methods

journal homepage: www.elsevier.com/locate/jneumeth

Neurofilament-histomorphometry comparison in the evaluation of unmyelinated axon regeneration following peripheral nerve injury: An alternative to electron microscopy

J. Michael Hendry[a,b,c,*], M. Cecilia Alvarez-Veronesi[a,d], Cameron Chiang[a], Tessa Gordon[a], Gregory H. Borschel[a,b,c,d]

[a] Division of Plastic and Reconstructive Surgery, The Hospital for Sick Children, 555 University Avenue, Toronto, ON, M5G 1X8, Canada
[b] Department of Surgery, University of Toronto, 149 College Street, 5th floor, Toronto, ON, M5T 1P5, Canada
[c] Institute of Medical Science, University of Toronto, 1 King's College Circle, Room 2374, Toronto, ON, M5S 1A8, Canada
[d] Institute of Biomaterials and Biomedical Engineering, University of Toronto, 164 College Street, Room 407, Toronto, ON, M5S 3G9, Canada

ARTICLE INFO

Keywords:
Electron microscopy
Peripheral nerve regeneration
Unmyelinated axons
Neurofilament

ABSTRACT

Background: Currently, assessment of unmyelinated axon regeneration is limited to electron microscopy (EM), which is expensive, time consuming and not universally available. This study presents a protocol to estimate the number of unmyelinated axons in a regenerating peripheral nerve without the need for electron microscopy.
New method: The common peroneal nerve of Sprague-Dawley rats was transected, repaired and regenerated for 4 weeks. Two distal adjacent segments of the regenerating nerve were then processed for either conventional histomorphometry using toluidine blue or immunolabeling of neurofilament protein. Myelinated axon and total axon counts were obtained, respectively, to generate estimates of unmyelinated axon numbers, which were then compared to unmyelinated axon counts using EM from the same specimens. For comparison, unmyelinated axons were counted in an uninjured rat laryngeal nerve.
Results: After 4 weeks of regeneration, the estimated number of regenerating unmyelinated axons was 4044 ± 232 using this technique, representing 81.3% of the total axonal population. By comparison, the proportion of unmyelinated axons in the uninjured laryngeal nerve was 55% of the total axonal population.
Comparison with existing method: These estimates correlate with electron microscopy measurements, both in terms of the proportion of unmyelinated axons and also by linear regression analysis.
Conclusions: The neurofilament staining method correlates with electron microscopy estimates of the same nerve sections. It is useful for the efficient counting of unmyelinated axons in the regenerating peripheral nerve and can be used by laboratories that do not have access to EM facilities.

1. Introduction

The peripheral nervous system retains the intrinsic capacity to regenerate unlike the central nervous system. This capacity to regenerate is limited however, by mechanical, physiological and molecular factors that various technologies can potentially manipulate to improve outcomes. Investigating new technologies and studying the natural history of peripheral nerve regeneration requires reliable metrics of evaluating both the extent of regeneration at the cellular level and also physiological functional recovery. Standard methods of investigation include histomorphometry, retrograde labeling, various microscopy and imaging techniques (Wood et al., 2011). These validated techniques enable counting of regenerating axons distally in a recovering nerve, the number of neurons that regenerate their axons, and the histologic patterns of nerve regeneration, respectively.

Histomorphometry is an established and validated technique (Hunter et al., 2007) based on toluidine blue staining of nerve cross-sections that allows for enumeration of total numbers of regenerated myelinated axons in a regenerating nerve. However, this technique does not provide information on patterns of unmyelinated fiber

Abbreviations: EM, electron microscopy; IHC, immunohistochemistry

* Corresponding author at: Division of Plastic and Reconstructive Surgery, Kingston Health Science Centre, Hotel Dieu Hospital Site, Brock 3, Rm. 389D, 166 Brock Street, Kingston, ON, K7L 5G2, Canada.
E-mail addresses: michael.hendry@kingstonhsc.ca (J.M. Hendry), mc.alvarezveronesi@gmail.com (M.C. Alvarez-Veronesi), cameron.d.chiang@gmail.com (C. Chiang), tessat.gordon@gmail.com (T. Gordon), gregory.borschel@sickkids.ca (G.H. Borschel).

https://doi.org/10.1016/j.jneumeth.2019.03.006
Received 14 November 2018; Received in revised form 2 March 2019; Accepted 5 March 2019
Available online 07 March 2019
0165-0270/

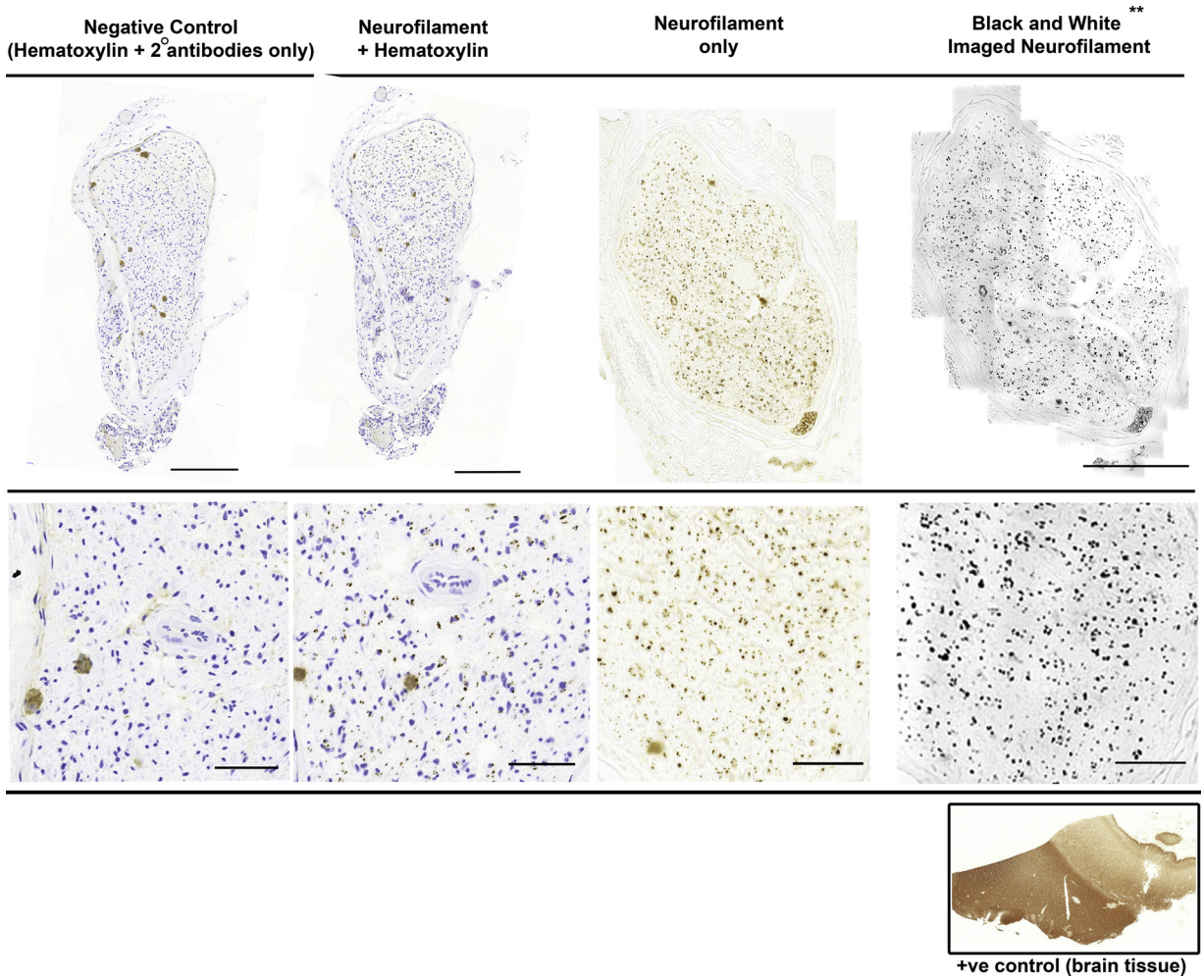

Fig. 1. Immunohistochemical procedure for generating total axon counts. Formalin fixed nerve sections 10 mm distal to the repair site stained for medium-chain neurofilament primary antibodies and counterstained with hematoxylin (left two columns). To produce colour images for hematoxylin and/or NF controls in the left 3 columns, slides were scanned using a 3DHistech Pannoramic 250 Flash II Scanner. Images were acquired using a Zeiss 20x/0.8 lens and a CIS VCC-FC60FR19CL camera, and stitched together in Adobe Photoshop. For counting purposes, no hematoxylin counterstain was used. This created a cloud of pigmented points (middle right column), which was imaged at 100x magnification in black and white (far right column) to allow counting of axons with semi-automated software (Image pro-analyzer). Scale bar represents 200 μm and 25 μm for the upper and lower rows, respectively.

regeneration. In fact, very little data exists in the literature on patterns of unmyelinated axon regeneration despite the large proportion of unmyelinated vs. myelinated axons in mammalian systems; with ratios ranging from 3:1 in cats to 9:1 in rabbits (Lisney, 1989). The proportion of unmyelinated to myelinated axons in humans is not known. Accordingly, there may be a wealth of valuable information to be gained by studying patterns of unmyelinated and total nerve fiber regeneration (ie: both myelinated and unmyelinated) in a variety of experimental settings. Furthermore, an improved understanding of unmyelinated axon regeneration may yield clinically relevant data regarding the development of pain as well as regeneration of sensory and autonomic nerves. Currently, assessment of unmyelinated axon regeneration is limited to electron microscopy (EM) which is both expensive, time-consuming and relies on extrapolated estimates of axon density based on multiple samples from a single nerve section (Geuna et al., 2000; Gunderson, 1978; Kaplan et al., 2010; Larsen, 1998; Raimondo et al., 2009).

We describe a new method for estimating unmyelinated and total (myelinated plus unmyelinated) axon counts within a regenerating nerve. The method is based on comparing immediately adjacent nerve cross sections in a regenerating nerve. Unmyelinated axon number is calculated as the difference between counts of total axon number (from neurofilament stained sections) and counts of myelinated axons (from toluidine blue stained sections). We show that this technique quantifies myelinated and unmyelinated axons in a regenerating peripheral nerve and that these counts correlate with those of electron microscopy. This technique is more widely accessible, less expensive and less time consuming than EM.

2. Materials and methods

A single cohort of 7 rats underwent surgical transection of their common peroneal (CP) nerves followed by immediate repair. All experimental rats were in the weight range of 250–300 g. All protocols used in this study were approved by the Hospital for Sick Children's Laboratory Animal Services Committee (Toronto, Canada), and adhered strictly to the Canadian Council on Animal Care guidelines.

2.1. Surgical model of nerve regeneration

The rats were anaesthetized with inhaled isofluorane gas and the plane of anesthesia titrated to respiratory rate. The bilateral hindlimbs were shaved from the greater trochanter to immediately distal to the knee. A skin incision was made 5 mm below a line connecting the greater trochanter and the knee joint, followed by blunt separation along the septum between the biceps femoris and the vastus lateralis

muscles to expose the sciatic nerve. Exposure was achieved from the hip to the knee joint and tissue retractors were inserted. The CP nerve was separated from the tibial (TIB) nerve using blunt dissection as far proximally as possible without compromising the epineurium. Approximately 5 mm distal to this bifurcation, the CP nerve was transected sharply with iris scissors followed by immediate repair using two epineurial 9-0 Nylon microsutures. The wound was closed in layers. Routine post-operative monitoring and analgesia with meloxicam (~ 0.5 mg/kg) was provided during recovery.

2.2. Tissue collection

After 4 weeks of regeneration, the same surgical approach was used to expose the repaired CP nerve under sterile conditions. The CP nerve was exposed and a 2 mm long segment removed 10 mm distal to the original repair site. This specimen was divided in half and the proximal 1 mm piece fixed in 2% solution of glutaraldehyde in preparation for histomorphometry processing. The distal 1 mm sample was fixed in 10% formalin in preparation for immunohistochemical processing.

2.3. Toluidine blue staining and myelinated axon counting with light microscopy

The histomorphometry samples were post-fixed with 1% osmium tetroxide, ethanol dehydrated, and embedded in Araldite 502 (Polyscience Inc., Warrington, PA). Semi-thin sections were cut using a LKB II Ultramicrotome (LKB-Produckter A.B., Broma, Sweden) and then stained with 1% toluidine blue for examination by light microscopy. At 100X overall magnification, a tiled composite image of the entire nerve cross-section was captured using Image-Pro Analyzer version 9.0 (Media Cybernetics, Rockville, MD) and the number of axons evaluated using semi-automated software designed in MatLab (Mathworks Inc, Natick, MA). These nerve cross-sections were evaluated for the total number of myelinated axons contained within them.

2.4. Neurofilament staining and total axon counting with light microscopy

The nerve sample for immunohistochemical analysis was fixed for a minimum of 48 h prior to processing and stained with neurofilament primary antibodies (Cedarlane Laboratories) (Fig. 1). The samples were processed by incubating in buffered formalin, graded ethanol dehydration, xylene and paraffin treatment. Processing was performed by a Leica Peloris tissue processor (Leica Biosystems, Saint Louis, MO). After processing, tissue was embedded in paraffin and sectioned at 4 μm with a Thermoscientific Micron HM-355 S Semi-automated microtome (Thermo Fisher Scientific, Inc.) and mounted on Fisher-Brand Superior Plus glass slides. Certain slides (controls) were counterstained with hematoxylin. For slides used in analysis, no counterstain was used, only chromagen labeled primary anti-neurofilament antibodies. Coverslipped slides were imaged to create black and white tiled images of entire nerve cross-sections at 100x magnification in a similar fashion to the histomorphometry sections. Axon counting was performed using Image-Pro Analyser software (MediaCybernetics, Rockville, Maryland).

Estimates of unmyelinated axon numbers were generated by counting total axon numbers from neurofilament stained sections (Fig. 2A & B) and subtracting the number of myelinated axons counted on histomorphometry (Fig. 2C).

2.5. Axon counting in uninjured nerve using electron microscopy

The laryngeal nerve of two Sprague Dawley rats were harvested for exhaustive manual counting of total myelinated and unmyelinated nerve fibers, the gold standard technique. The laryngeal nerve was chosen as it is a small, mixed motor and sensory nerve with a diameter of approximately 200 μm, where all nerve fibers can be practically counted within a tiled composite image. A 2 mm segment of laryngeal nerve was harvested and fixed in 2% glutaraldehyde solution, post-fixed with osmium tetroxide, sectioned, mounted on a Formvar support, and stained with lead citrate. Tiled composite images were generated at 5000x magnification by splicing individual frames together using Adobe Photoshop, version CS3 (Adobe Inc.) (Fig. 3A & B). Individual myelinated and unmyelinated nerve fibers were counted directly from these images.

2.6. Axon counting in regenerating nerve using electron microscopy

The 4-week regenerated nerve specimens were processed in a similar fashion to those described above, except that these sections were mounted on a 200-slot mesh grid. Images at 3000x magnification were captured at regular intervals, centered within every third frame of the slot-mesh to replicate the conditions of an unbiased counting frame. These images were calibrated to scale, axons were counted within the sampling frame and density estimates derived from each image. Consistent with stereological principles, all axon profiles in contact with the lower and left margin of the frame were included with the count and those touching the right and upper margin were excluded. The mean myelinated and unmyelinated axon density was calculated from 6 to 7 individual images for each section. Myelinated and unmyelinated axon numbers were then calculated by multiplying the mean axon density by the cross-sectional area of the specimen.

2.7. Statistical analysis

Standard descriptive statistics including mean and standard error the mean were used to compare nerve fiber numbers between groups. EM and neurofilament staining derived estimates of unmyelinated nerve fiber numbers were compared using a linear regression analysis. Statistical comparison between electron microscopy and neurofilament-stained estimates was carried out using a paired Student's *t*-test.

3. Results

Seven regenerating common peroneal (CP) nerves in the rat were prepared and processed to estimate the number of unmyelinated nerve fibers using stains for toluidine blue and neurofilament. Nerve cross-sections from these rats were then prepared for electron microscopy (EM) for statistical comparison. Three rat laryngeal nerves were first used to quantify the relative proportions of myelinated and unmyelinated axons in an uninjured mixed sensory and motor nerve using the gold standard technique, directly counting all axons with EM.

A single tiled composite image was created for each laryngeal nerve cross section, which was used to directly count each myelinated and unmyelinated axon. These tiled composite images revealed heterogeneity in nerve fiber morphology with respect to size and myelination (Fig. 3A). Unmyelinated axons were readily observed at 5000x magnification, featuring axoplasm, smaller size, frequent mitochondria and no myelin (Fig. 3B). We observed that the absolute number of axons varied in proportion to the size of the nerve, but the proportion of myelinated to unmyelinated fibers was similar. The mean proportion of myelinated axons was 44.6 ± 4.1% (± SEM) and the mean proportion of unmyelinated axons was 55.4 ± 4.1% in an uninjured rat laryngeal nerve (Fig. 3C).

Black and white whole-section composite images of neurofilament-stained cross-sections were compared with toluidine blue stained cross-sections from the same nerve. There was an increased density of the axons stained with neurofilament compared with the myelinated nerve fibers observed in histomorphometric cross-sections (Fig. 2B and C). This comparison was quantified by subtracting the number of myelinated nerve fibers (histomorphometry sections) from the total number of neurofilament stained axons; the difference representing the estimate of unmyelinated fiber numbers for each nerve (Fig. 4A). Using this technique the estimated mean number of unmyelinated axons in the 4-

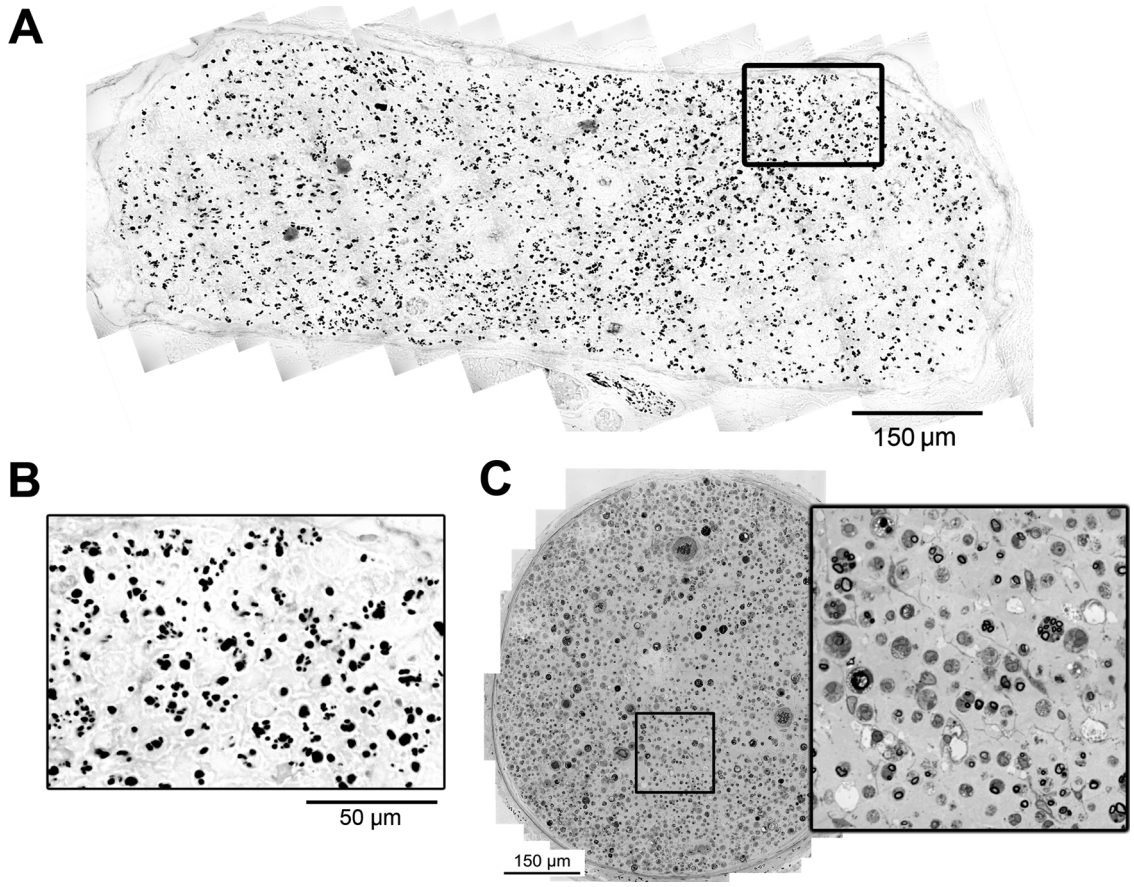

Fig. 2. Tiled composite images of neurofilament stained common peroneal nerve sections are compared with conventional histomorphometry. Semi-thin nerve cross sections 10 mm distal to the repair site were harvested 4 weeks after repair and immunostained for neurofilament. (A) Representative complete tiled image of whole nerve cross-sections. (B) Magnified image of area outlined in 'A' depicting individual axons that have regenerated 4 weeks after immediate repair. (C) Sections from an immediately adjacent segment of regenerating nerve were processed in glutaraldehyde for conventional histomorphometry against which total axon counts from A were compared. Note that orienting these minute specimens for paraffin embedding during IHC staining led to a somewhat flattened appearance of otherwise true cross sections.

week regenerating CP nerve in this sample was 4044 ± 232 (± SEM). The relative proportion of unmyelinated axons at this time point (˜83%) in regeneration is considerably increased compared with the uninjured laryngeal nerve (˜55%) and those values published in the literature (62–67%) (Jenq et al., 1987; Jenq and Coggeshall, 1985; Toft et al., 1988). These proportions were consistent between both neurofilament estimates and EM estimates of the same nerve sections after 4 weeks of regeneration (Fig. 4B).

Estimates from this neurofilament-histomorphometry technique were compared statistically with EM estimates from the same sections. We observed that these two techniques correlated well through linear regression in estimating the number of unmyelinated axons (Fig. 5A). However, each technique produced different values for the estimated number of unmyelinated axons. Similarly, myelinated axon estimates from EM cross-sections correlated directly with the total numbers of myelinated axons counted with histomorphometry (gold standard) ($r = 0.61$); however, they differed in their absolute number (Fig. 5B). This difference was significant when compared with a paired Student's *t*-test (Fig. 5D). Comparison of unmyelinated axon density yielded numbers that were more similar in absolute value (Fig. 5C), which raises the question of whether surface area and subtle processing differences accounts for the discrepancy.

4. Discussion

This study was successful in establishing a protocol for efficiently counting the number of unmyelinated axons in a cross-section of a regenerating nerve, a measurement currently under-reported in the literature. This technique relies on a comparison between a neurofilament antibody-stained section (myelinated and unmyelined axons) and toluidine blue stained sections (myelinated axons only) from immediately adjacent positions along the length of a repaired peripheral nerve (Figs. 1, 2 and 4). This technique is best applied to regenerating nerves and not uninjured nerves, as the latter can have high density of all fiber types that may cause confluent staining of neurofilament antibody and obscured counts.

These estimates of unmyelinated common peroneal (CP) nerve regeneration were compared with the ratios of myelinated to unmyelinated axons in an uninjured rat laryngeal nerve (Fig. 3). The rat laryngeal nerve was selected as it has both sensory function to the rat glottis, motor innervation to the laryngeal musculature and is small enough to allow for a composite tiled image of its full cross sectional area (Hishida et al., 1997; Rhee et al., 2004). Furthermore, the ratio of myelinated to unmyelinated fibers in the uninjured laryngeal nerve was not substantially different (49% : 51%) to the ratio found in the uninjured common peroneal nerve (36% : 64%) (Hishida et al., 1997; Jenq et al., 1987). To support the reproducibility of our EM technique, the number of myelinated laryngeal nerve axons observed in this study (605) was also consistent with values published in the literature (Lima et al., 2007).

Little data exists on the relative proportion of myelinated and unmyelinated fibers in the regenerating nerve. In this study, we observed that the number of unmyelinated axons in the laryngeal nerve was approximately 55% of the total axonal population (Fig. 3), similar to

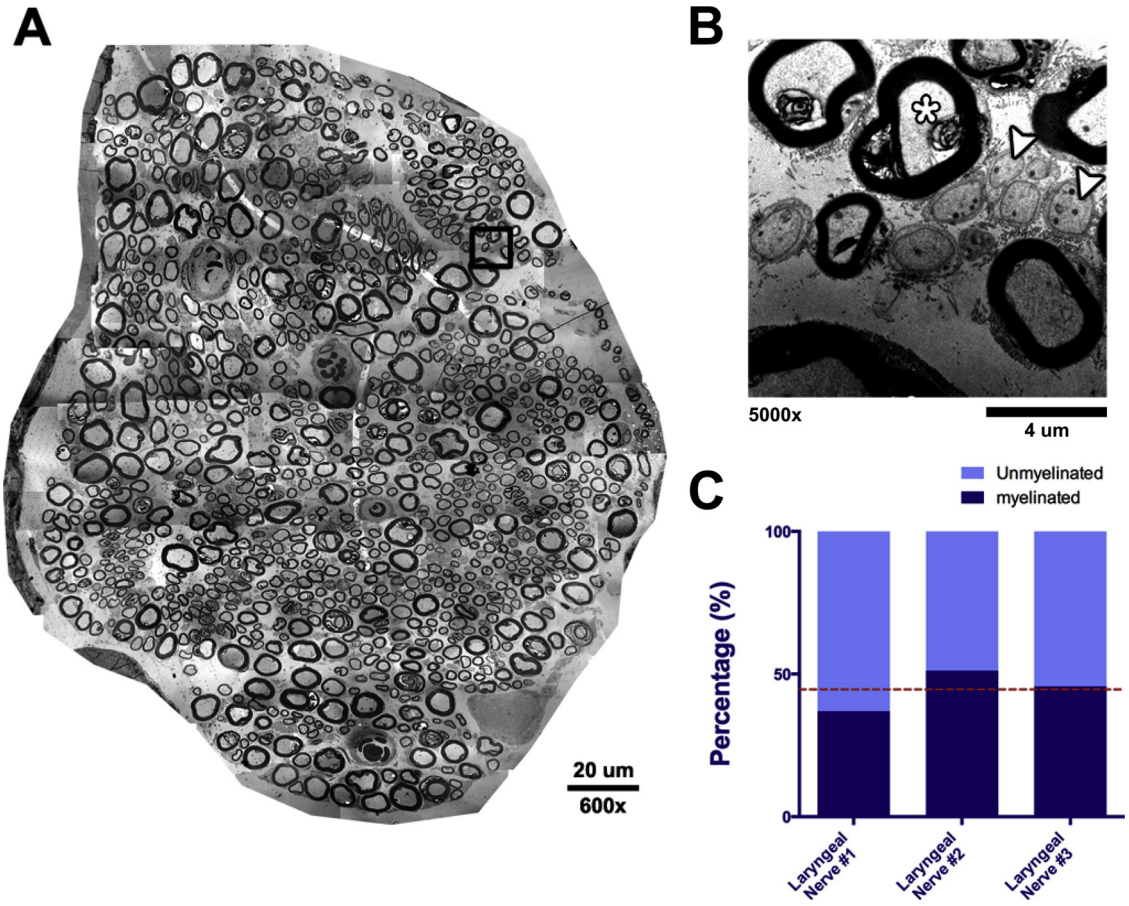

Fig. 3. Direct counting of all myelinated and unmyelinated axons from tiled composite images of uninjured rat laryngeal nerve sections reveal a substantial proportion of unmyelinated axons. A) Tiled composite electron microscopy image of the rat laryngeal nerve. B) Higher magnification view of region highlighted in A which reveals many unmyelinated (arrowhead) and myelinated fibers (asterisk). C) Representative proportions of myelinated and unmyelinated fibers counted exhaustively in tiled composite images of uninjured rat laryngeal nerve branches. Note that the mean number (red dashed line) of unmyelinated axons in these sections comprises 55% of the total axonal population.

those published in the literature (51%) (Hishida et al., 1997). Four weeks after transection and repair of the common peroneal nerve, the proportion of unmyelinated axons increased considerably in the distal nerve stump, accounting for 83% of the total fiber population. This proportion represents an increase in approximately 20% from the pre-injury ratio reported in the literature and substantial change from the ratio observed in the laryngeal nerve sections (Fig. 4). Very few studies were identified that quantified this relationship.

The proportion of unmyelinated axons that comprise a peripheral nerve is substantial (˜55% uninjured laryngeal nerve; ˜83% of early regenerating common peroneal nerve). This large population of unmyelinated nerve fibers, many of which are cutaneous sensory nerve fibers, further emphasize the importance of obtaining a better understanding of their patterns of regeneration. The patterns of regeneration

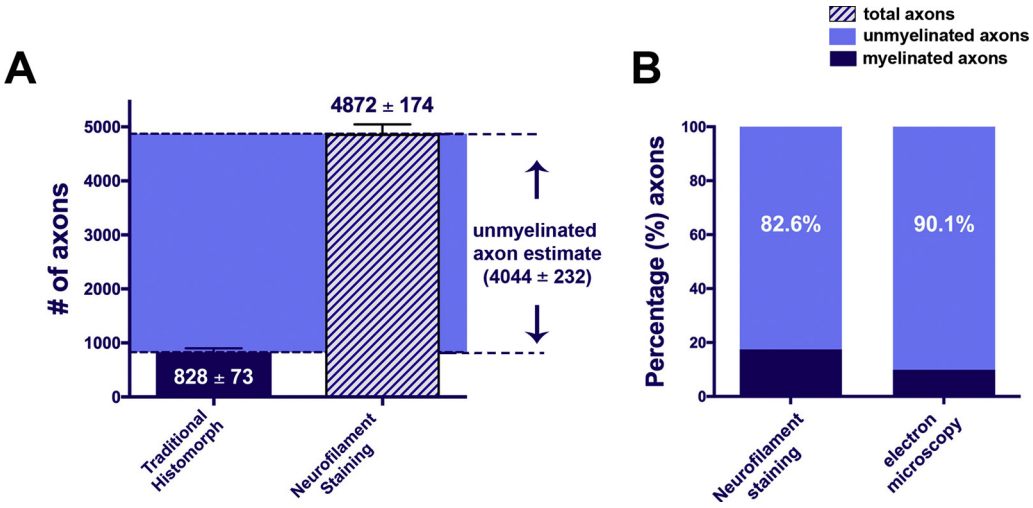

Fig. 4. Estimates of unmyelinated nerve fibers in the 4 week regenerating common peroneal nerve using the neurofilament-histomorphometry comparison method. (A) Unmyelinated nerve fiber number estimates are represented by the arithmetic difference of the total nerve fiber count and the myelinated nerve fiber count derived from histomorphometry. (B) The percentage of unmyelinated nerves in the total nerve population is substantial and correlates well with EM estimates derived from the same population.

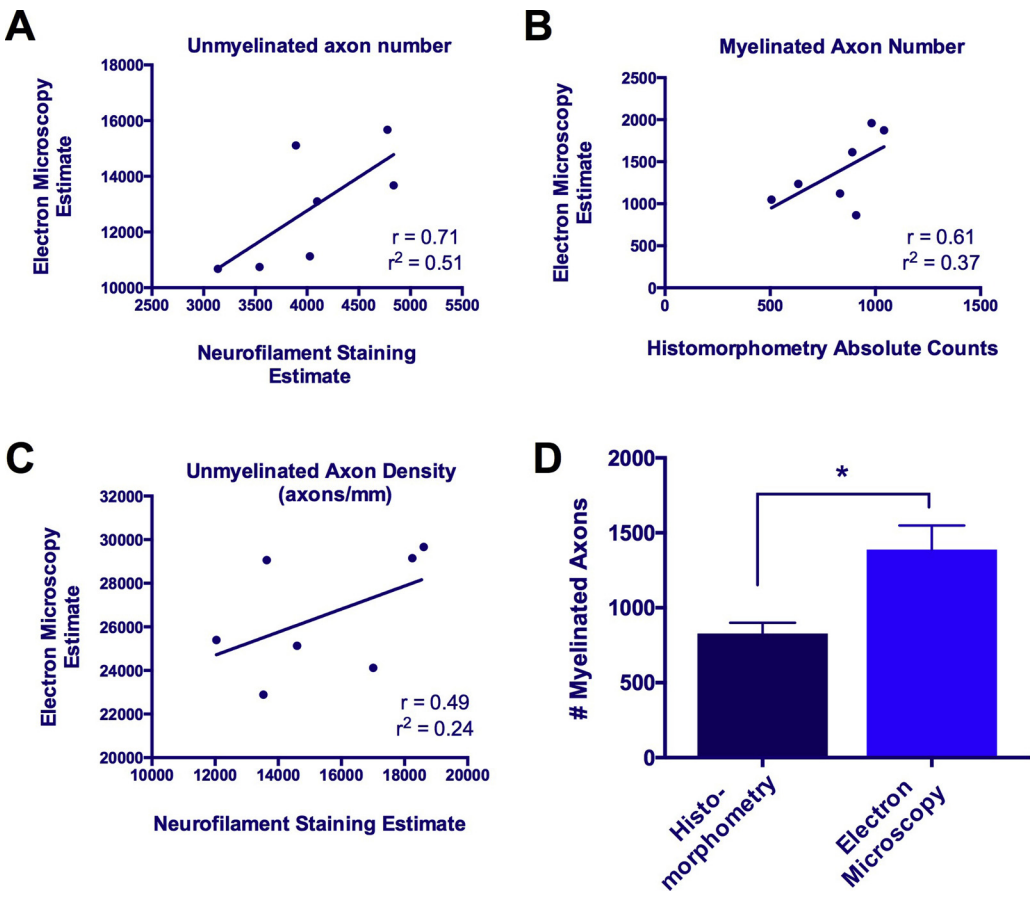

Fig. 5. Comparison between neurofilament-histomorphometry technique and electron microscopy when examining myelinated and unmyelinated axons counts in the recovering peroneal nerve. (A) Unmyelinated axon counts from the same nerve specimen were obtained using the two different techniques and compared. Good correlation was observed by linear regression. (B) Electron microscopy (EM) estimates were compared with the 'true' number of myelinated nerve fibers and found to correlate well on linear regression. (C) Unmyelinated nerve fiber density with the two techniques did not correlate as well, perhaps due to differences in embedding technique; (D) EM estimates of myelinated nerve fiber number were significantly different from the 'true' numbers derived from toluidine blue stained sections.

in unmyelinated axons are not well studied. Ratios of myelinated to unmyelinated axon numbers will vary between species and function of the nerve, ranging from 1:0.4 (rat muscle) to 1:9 in rabbit (Jenq and Coggeshall, 1985; Lisney, 1989). Data for similar ratios in the rat are sparse. Jenq and Coggeshall (1985) examined proportions of myelinated and unmyelinated axons regenerating across a nerve gap and noted that proportions of axon populations was strongly influenced by the function of the nerve. In this study, the pre-injured rat laryngeal nerve contained a ratio of 1:1.3 (myelinated: unmyelinated nerve fibers) and the early regenerating CP nerve contained a ratio of 1:9. This relative increase in unmyelinated axon number may be explained by preferential axonal sprouting of unmyelinated axons compared with myelinated ones distal to the repair site. Interestingly, distal axonal sprouting and similar ratios of myelinated:unmyelinated axons (1:10) were observed after 4 weeks in a rat peroneal nerve crush model (Toft et al., 1988), consistent with findings in this study.

Unmyelinated axon numbers were calculated as the difference between total axon counts from neurofilament-stained nerve cross-sections and myelinated axon counts from toluidine blue stained sections. Estimates of axon number obtained from these two methods correlated statistically with a moderately strong r-value of 0.71 and 0.61 for unmyelinated and myelinated axon counts, respectively. Specifically, nerve cross sections with greatest number of axons tended to have the highest counts using either technique. (Fig. 5). However, the absolute axon counts for the estimates derived by these two methods were significantly different by paired *t*-test comparison (Fig. 5). Interpretation of this discrepancy is difficult considering that there is no consistently agreed upon values reported in the literature. The few instances where unmyelinated axon number is quantified in the distal common peroneal nerve post-repair range broadly from 2170 to 10,011 (Jenq et al., 1987; Toft et al., 1988). Electron microscopy techniques in these studies varied greatly. There are several possible factors that contribute to this observed variation in this study. Morphological bias, defined as the over representation of smaller objects within large sample size areas (Geuna et al., 2000), may have contributed to this overestimation in our electron microscopy technique. Further, underestimation of neurofilament counts may have contributed due to coalescence of chromagen signal when unmyelinated axons were closely packed together. Embedding technique is also known to influence the density of countable structures, especially at the periphery of sections, biasing counting techniques like the 2D optical dissectors by as much as 25% (Deniz et al., 2018; Gardella et al., 2003).

Stereology of the peripheral nervous system aims to determine the number and the morphological characteristics of regenerating nerve fibers (Kaplan et al., 2010). Stereological techniques have evolved over time. These include the 'ratio technique' that multiplies axon density within a sample area by cross sectional area of the section (Kupfer et al., 1967; Mayhew, 1988), fractionator techniques to overcome inherent bias (Deniz et al., 2018; Gundersen, 1986; Mayhew, 1988), unbiased counting frames (Canan et al., 2008; Gunderson, 1978; Larsen, 1998) and semiautomated software techniques (Hunter et al., 2007). Such stereological techniques however, are nonetheless confounded by their own sources of error that are influenced by such factors as size and morphological recognition of cellular anatomy, species of animal, the embedding technique and tissue deformation, and the size of the sampling area (Deniz et al., 2018; Farel, 2002; Gardella et al., 2003; Kaplan et al., 2010; von Bartheld et al., 2017).

There has been much debate over which of these stereological methods is the most ideal (Farel, 2002; Raimondo et al., 2009). The most straightforward and accurate method is to directly count all nerve fibers in a cross-section (Farel, 2002). However, given their small size and lack of myelin, counting all unmyelinated axons would rely on electron microscopy. At present, the use of electron microscopy is limited to qualitative observations of nerve ultrastructure to

complement enumeration by other means (Gomez-sanchez et al., 2017; Hoben et al., 2018; Rui et al., 2018), generating estimates of unmyelinated axon density without extrapolation to whole nerve counts (Duchesne et al., 2016) and high throughput enumeration of myelinated axons (Bond and Parkinson, 2018). Directly counting all unmyelinated axons in a nerve cross-section using electron microscopy would be prohibitively time and labor intensive. Accordingly, this reality has limited our study of unmyelinated axon regeneration, until now.

This study presents an efficient method of enumerating both total and unmyelinated nerve fiber populations by directly counting all regenerating myelinated and unmyelinated axons. This technique avoids the extrapolations and bias inherent in many of the stereological techniques employed today. Previous attempts at using neurofilament staining to characterize nerve regeneration across a whole nerve cross-section led to rapid enumeration, but no critical discrimination between myelinated and unmyelinated nerve fiber populations (Heijke et al., 2000). The technique presented here uses a simple comparison between neurofilament and toluidine blue stained nerve sections. The advantage beyond simply estimating unmyelinated axon number is that the investigator can still derive all the conventional metrics of histomorphometry, such as myelin thickness and G-ratio. The assumptions made in this technique are that the number of axons does not change in a clinically significant way in the ˜ 1 mm interval between sections and that there is no difference in total axon number when resin (EM/toluidine blue) vs paraffin (immunohistochemistry) is used for embedding (Raimondo et al., 2009). This technique was validated against EM estimates of the same slides. While the EM estimates tended to be higher than expected for reasons discussed above, the strengths of the sampling strategy included systematic unbiased sampling using slot mesh grid placed randomly across the nerve cross-section.

5. Conclusions

This study presents a novel imaging protocol to estimate unmyelinated axon number that avoids extrapolating small sample estimates from within a heterogeneous regenerating nerve cross section. Further, it provides a method to measure unmyelinated nerve regeneration without the need for EM which can be expensive, time consuming and have limited accessibility. The value of this technique may be viewed as a repurposing of common laboratory stains to measure something once limited to electronic microscopy. This is more resource efficient and less costly. Further, this study quantified myelinated and unmyelinated nerve fiber numbers in the regenerating rat CP nerve, data that is scarcely reported elsewhere in the literature.

Declarations of interest

None.

Acknowledgments

This work would not have been possible without the experience and skill of Yew-Meng Heng, the electron microscopist at The Hospital for Sick Children. This work was supported by the Canadian Institute for Health Research grant MOP-114950 and support provided through the Hospital for Sick Children, Toronto, Ontario.

References

Bond, P., Parkinson, D.B., 2018. The use of low vacuum scanning electron microscopy (LVSEM) to analyze peripheral nerve samples. In: Monje, P.V., Kim, H.A. (Eds.), Schwann Cells: Methods and Protocols. Springer New York, New York, NY, pp. 349–357. https://doi.org/10.1007/978-1-4939-7649-2_23.

Canan, S., Bozkurt, H.H., Acar, M., Vlamings, R., Aktas, A., Sahin, B., Temel, Y., Kaplan, S., 2008. An efficient stereological sampling approach for quantitative assessment of nerve regeneration. Neuropathol. Appl. Neurobiol. 34, 638–649. https://doi.org/10.1111/j.1365-2990.2008.00938.x.

Deniz, Ö.G., Altun, G., Kaplan, A.A., Yurt, K.K., Von Bartheld, C.S., Kaplan, S., 2018. A concise review of optical, physical and isotropic fractionator techniques in neuroscience studies, including recent developments. J. Neurosci. Methods 310, 45–53. https://doi.org/10.1016/j.jneumeth.2018.07.012.

Duchesne, M., Magy, L., Richard, L., Ingrand, P., Neau, J., Mathis, S., Vallat, J.-M., 2016. Simultaneous quantification of unmyelinated nerve fibers in Sural Nerve and in skin. J. Neuropathol. Exp. Neurol. 75, 53–60. https://doi.org/10.1093/jnen/nlv005.

Farel, P.B., 2002. Trust, but verify: the necessity of empirical verification in quantitative neurobiology. Anat. Rec. 269, 157–161. https://doi.org/10.1002/ar.10111.

Gardella, D., Hatton, W.J., Rind, H.B., Rosen, G.D., von Bartheld, C.S., 2003. Differential tissue shrinkage and compression in the z-axis: implications for optical disector counting in vibratome-, plastic- and cryosections. J. Neurosci. Methods 124, 45–59. https://doi.org/10.1016/S0165-0270(02)00363-1.

Geuna, S., Tos, P., Battiston, B., Guglielmone, R., 2000. Verification of the two-dimensional disector, a method for the unbiased estimation of density and number of myelinated nerve fibers in peripheral nerves. Ann. Anat. 182, 23–34. https://doi.org/10.1016/S0940-9602(00)80117-X.

Gomez-sanchez, J.A., Pilch, K.S., Van Der Lans, M., Fazal, S.V., Benito, C., Wagstaff, L.J., Mirsky, R., Jessen, K.R., 2017. After nerve injury, lineage tracing shows that myelin and Remak Schwann Cells elongate extensively and branch to form repair Schwann Cells. Which Shorten Radically on Remyelination. J. Neurosci. 37, 9086–9099. https://doi.org/10.1523/JNEUROSCI.1453-17.2017.

Gundersen, H.J.G., 1986. Stereology of arbitrary particles. A review of unbiased number and size estimators and the presentation of some new ones. in memory of William R. Thompson. J. Microsc. 143, 3–45.

Gunderson, H.J.G., 1978. Estimators of the number of objects per unit area unbiased by edge effects. Microsc. Acta 81, 107–117.

Heijke, G.C.M., Klopper, P.J., Baljet, B., Van Doorn, I.B.M., Dutrieux, R.P., 2000. Method for morphometric analysis of axons in experimental peripheral nerve reconstruction. Microsurgery 20, 225–232. https://doi.org/10.1002/1098-2752(2000)20:5<225::AID-MICR3>3.0.CO;2-S.

Hishida, N., Tsubone, H., Sugano, S., 1997. Fiber composition of the superior laryngeal nerve in rats and Guinea Pigs. J. Vet. Med. Sci. 59, 499–501.

Hoben, G.M., Ee, X., Schellhardt, L., Yan, Y., Hunter, D.A., Moore, A.M., Snyder-warwick, A.K., Stewart, S., Mackinnon, S.E., Wood, M.D., 2018. Increasing nerve autograft length increases senescence and reduces regeneration. Plast. Reconstr. Surg. 142, 952–961. https://doi.org/10.1097/PRS.0000000000004759.

Hunter, D.A., Moradzadeh, A., Whitlock, E.L., Brenner, M.J., Myckatyn, T.M., Wei, C.H., Tung, T.H.H., Mackinnon, S.E., 2007. Binary imaging analysis for comprehensive quantitative assessment of peripheral nerve. J. Neurosci. Methods 166, 116–124. https://doi.org/10.1016/j.jneumeth.2007.06.018.

Jenq, C.B., Coggeshall, R.E., 1985. Long-term patterns of axon regeneration in the sciatic nerve and its tributaries. Brain Res. 345, 34–44.

Jenq, C., Jenq, L.E., Coggeshall, R.E., 1987. Numerical patterns of axon regeneration that follow sciatic nerve crush in the neonatal rat. Exp. Neurol. 95, 492–499.

Kaplan, S., Geuna, S., Ronchi, G., Ulkay, M.B., von Bartheld, C.S., 2010. Calibration of the stereological estimation of the number of myelinated axons in the rat sciatic nerve: a multicenter study. J. Neurosci. Methods 187, 90–99. https://doi.org/10.1016/j.jneumeth.2010.01.001.

Kupfer, C., Chumbley, L., Downer, J.D.C., 1967. Quantitative histology of optic nerve, optic tract and lateral geniculate nucleus of man. J. Anat. 101, 393–401.

Larsen, J.O., 1998. Stereology of nerve cross sections. J. Neurosci. Methods 85, 107–118.

Lima, N.T., Fazan, V.P., Colafemina, J.F., Barreira, A.A., 2007. Recurrent laryngeal nerve post-natal development in rats. J. Neurosci. Methods 165, 18–24. https://doi.org/10.1016/j.jneumeth.2007.05.012.

Lisney, S.J.W., 1989. Regeneration of unmyelinated axons after injury of mammalian peripheral nerve. Q. J. Exp. Physiol. 74, 757–784.

Mayhew, T.M., 1988. An efficient sampling scheme for estimating fibre number from nerve cross sections: the fractionator. J. Anat. 157, 127–134.

Raimondo, S., Fornaro, M., Di Scipio, F., Ronchi, G., Giacobini-Robecchi, M.G., Geuna, S., 2009. Methods and protocols in peripheral nerve regeneration experimental research. Part II-morphological techniques. Int. Rev. Neurobiol. 87, 81–103. https://doi.org/10.1016/S0074-7742(09)87005-0.

Rhee, H.S., Lucas, C.A., Hoh, J.F.Y., 2004. Fiber types in rat laryngeal muscles and their transformations after denervation and reinnervation. J. Histochem. Cytochem. 52, 581–590.

Rui, J., Xu, Y.-L., Zhao, X., Li, J.-F., Gu, Y.-D., Lao, J., 2018. Phrenic and intercostal nerves with rhythmic discharge can promote early nerve regeneration after brachial plexus repair in rats. Neural Regen. Res. 13, 862–868. https://doi.org/10.4103/1673-5374.232482.

Toft, P., Fugleholm, K., Schmalbruch, H., 1988. Axonal branching following crush lesions of peripheral nerves of rat. Muscle Nerve 11, 880–889.

von Bartheld, C.S., Bahney, J., Herculano-Houzel, S., 2017. The search for true numbers of neurons and glial cells in the human brain: a review of 150 years of cell counting. J. Comp. Neurol. 524, 3865–3895. https://doi.org/10.1002/cne.24040.The.

Wood, M.D., Kemp, S.W.P., Weber, C., Borschel, G.H., Gordon, T., 2011. Outcome measures of peripheral nerve regeneration. Ann. Anat. 193, 321–333. https://doi.org/10.1016/j.aanat.2011.04.008.